sustainability

MDPI

Article

Spatiotemporal Analysis of Water Resources in the Haridwar Region of Uttarakhand, India

Shray Pathak [1,*], Chandra Shekhar Prasad Ojha [2], Rahul Dev Garg [2], Min Liu [1], Daniel Jato-Espino [3,*] and Rajendra Prasad Singh [4]

1 Key Laboratory of Geographical Information Sciences, Ministry of Education, and School of Geographic Sciences, Institute of Eco-Chongming, East China Normal University, Shanghai 200241, China; mliu@geo.ecnu.edu.cn
2 Department of Civil Engineering, Indian Institute of Technology Roorkee, Uttarakhand 247667, India; c.ojha@ce.iitr.ac.in (C.S.P.O.); rdgarg@ce.iitr.ac.in (R.D.G.)
3 Department of Transport and Projects and Processes Technology, Universidad de Cantabria, Av. de los Castros 46, 39005 Santander, Spain
4 School of Civil Engineering, Southeast University, Nanjing 210096, China; rajupsc@seu.edu.cn
* Correspondence: shraypathak@gmail.com (S.P.); daniel.jato@unican.es (D.J.-E.)

Received: 19 August 2020; Accepted: 10 October 2020; Published: 14 October 2020

Abstract: Watershed management plays a dynamic role in water resource engineering. Estimating surface runoff is an essential process of hydrology, since understanding the fundamental relationship between rainfall and runoff is useful for sustainable water resource management. To facilitate the assessment of this process, the Natural Resource Conservation Service-Curve Number (NRCS-CN) and Geographic Information Systems (GIS) were integrated. Furthermore, land use and soil maps were incorporated to estimate the temporal variability in surface runoff potential. The present study was performed on the Haridwar city, Uttarakhand, India for the years 1995, 2010 and 2018. In a context of climate change, the spatiotemporal analysis of hydro meteorological parameters is essential for estimating water availability. The study suggested that runoff increased approximately 48% from 1995 to 2010 and decreased nearly 71% from 2010 to 2018. In turn, the weighted curve number was found to be 69.24, 70.96 and 71.24 for 1995, 2010 and 2018, respectively. Additionally, a validation process with an annual water yield model was carried out to understand spatiotemporal variations and similarities. The study recommends adopting water harvesting techniques and strategies to fulfill regional water demands, since effective and sustainable approaches like these may assist in the simultaneous mitigation of disasters such as floods and droughts.

Keywords: water resources management; urban sprawl; rainfall-runoff modeling; spatiotemporal variation

1. Introduction

Water assets are the most essential renewable resources required by inhabitants in all forms. Thus, the consumption of water resources needs an effective decision planning for handling both its quality and quantity by considering its spatiotemporal variations. Land use and land cover (LULC) classification describes the role of human beings in affecting the land-cover patterns with time, which ultimately reflects the amount of surface runoff that different types of surface can deal with [1].

Cities experience high surface flows when the ratio of rainfall to infiltration rate is higher [2]. The amount of runoff generated depends upon LULC, soil properties, topography, slope, vegetation cover and atmospheric conditions [3–8]. The estimation and storage of stormwater is an essential component in the hydrological cycle to maintain the equilibrium in the city. Estimating surface

runoff is essential and plays an important role in hydrological engineering, modeling, and its related applications such as water balance calculation and flood design [9–11]. However, accounting for the spatiotemporal variability of runoff is complex, as it is governed by different hydrological parameters.

The National Resources Conservation Service-Curve Number (NRCS-CN) method, commonly known as the Soil Conservation Service-Curve Number (SCS-CN) method, was developed by the National Resource Conservation Service United State Department of Agriculture (USDA) in 1976. It is a reliable and straightforward method for estimating surface runoff from rainfall by obtaining curve number maps [12–19]. This approach is a direct function of the composite curve number (CN) to estimate the fraction of rainfall that flows as surface runoff [20,21]. High-resolution images help in computing the CN spatially to further estimate water flows within cities [22–27]. The role of the NRCS-CN model, including its concept, application, capabilities and limitations are clearly described in the scientific literature [28,29].

The conventional approach to compute CN for any catchment is to use available curves and tables, which is tedious and time consuming [9,20,30]. However, the implementation of this technique at the gridded scale by using GIS software becomes easier and takes less time [31–34]. The output generated in the gridded format is more reliable, provides detailed assessment and helps in developing strategic decision planning [35–40]. Globally, many studies have been performed using GIS techniques to simulate surface runoff [14,41–46]. A research focused on the Bebas river in Madha Pradesh yielded strong correlations between measured and simulated runoff depths using a GIS-based SCS-CN model [47]. Furthermore, the CN was applied to the Indian conditions using SCS-CN and GIS techniques to estimate spatial hydrological parameters and temporal variables [48]. In another study, GIS and remote sensing are concluded to be powerful tools for estimating runoff depth generation in the geo-hydrological environment [49]. Additionally, eight different models were combined with the SCS-CN model to calculate the accuracy of surface runoff depth estimates for 15 watersheds in Korea [50]. This technique was also utilized to identify and artificially recharge water harvesting structures [51–54].

Furthermore, similar parameters are required by other hydrological models such as Natural Capital Project's Integrated Valuation of Ecosystem Services and Tradeoffs model (InVEST) to estimate spatial water yield [55,56]. This model is developed based on the Budyko theory and consists of different tools for ecosystem assessment. To understand the role of meteorological parameters, the InVEST model has been applied both for extreme dry and wet conditions [57]. Additionally, it has been used to study different scenarios of urban sprawl and climate change in the watersheds of northwestern Oregon state [58], as well as to quantify sediment retention, water yield, carbon sequestration, and habitat quality under future land-use scenarios [59]. Pathak et al. [60] analyzed and validated the model for different watersheds varying in topographic characteristics. In urban areas, a major issue is to identify and locate suitable sites by considering socio-economic aspects of suitability [61]. Strategized policies are based on short-term scenarios and have low potential to handle extreme scenarios. The advancements in GIS tools have the capability to locate suitable sites for water harvesting and implement conservation practices [62]. Integrated geospatial technologies are essential to obtain updated information on LULC, soil texture, hydrologic soil groups and spatial rainfall variation to estimate surface runoff [63–68]. Calibration and validation of surface runoff models are very important to minimize uncertainty in the observed modeling inputs [69]. Additionally, public participation is involved through crowdsourcing along with stakeholders and water planners for an effective decision-making process [70].

Furthermore, an effective decision planning at a city scale is based on analyzing both the spatial and temporal variability of the water potential of the region. Long-term planning requires the evaluation of the spatiotemporal trend of surface runoff corresponding to rainfall. In this context, the analysis of variations in LULC is essential. If a stronghold is established on previous records, this kind of assessment could contribute to improving decision-making processes related to the management of water related disasters. Thus, the objective of the present study is twofold: to observe the effect of

the spatiotemporal variations of rainfall on surface runoff due to changes in the curve number and to ascertain the applicability and effectiveness of incorporating the NRCS-CN method into geospatial tools. The study also evaluates the temporal effect of anthropogenic activities on spatial surface runoff for the study region, Haridwar, India. This will assist water planners to identify suitable zones for artificially recharge aquifers or water harvesting structures in the region.

2. Study Area

The study area considered is Haridwar city, Uttarakhand, India. It is one of the seven holiest places to Hindus. Hence, it is essential to estimate water yield availability and the effect of anthropogenic activities, since the area is visited by millions of devotees worldwide. Consequently, the analysis was performed to understand the temporal impact on the landscape of the study region, which is represented in Figure 1. The geophysical characterization of the study region is described in subsequent sub-sections.

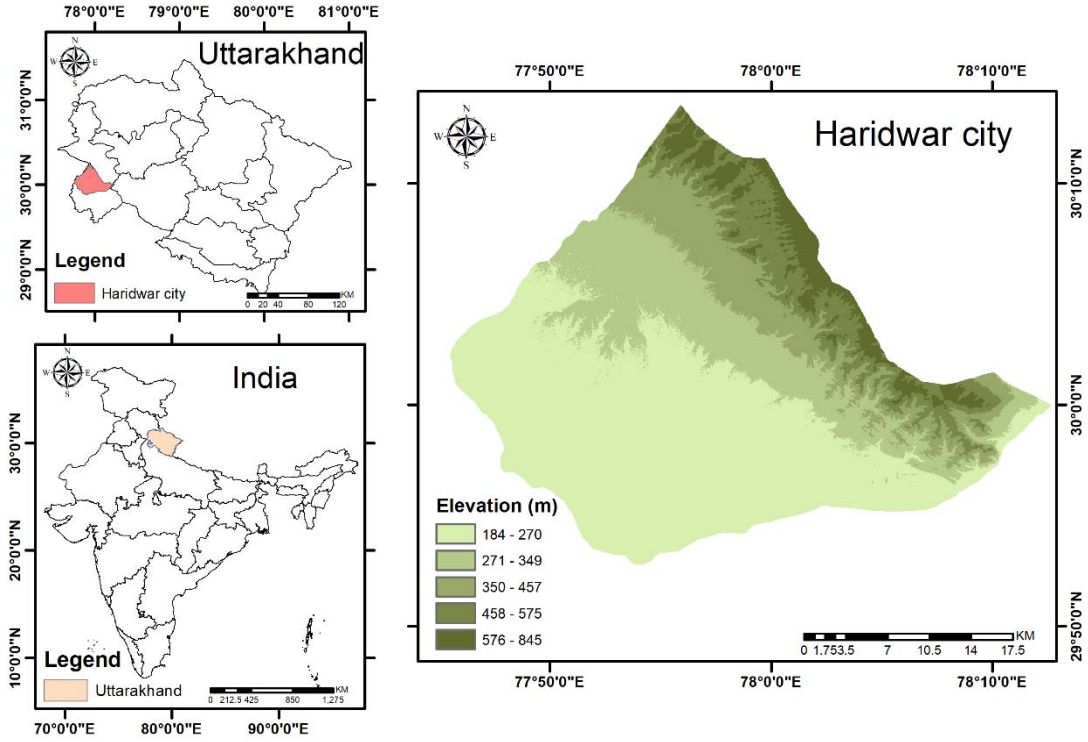

Figure 1. Geographical representation of the Haridwar city, India.

The Haridwar district is extended up to an area of about 2400 sq. km and located in the southwest part of the Uttarakhand state, India. Haridwar is at the height of 316 m above the mean sea level and lies within the North and Northeast of the Shivalik hills and the Ganges River in the South. The whole area is divided into four parts: mountainous region, upper bajada, lower bajada and alluvial plain. Major land-use classes in the study area are urban, agricultural, forest and barren land. Most of the study area (35% approximately) is forest. Moderate growth is observed, especially in roads and urban classes, as observed in 2018.

The study of climate data indicated that this area corresponds to a moderate subtropical humid region with a temperature drop in March (29.1 °C) that begins to rise until reaching its maximum in May (39.2 °C). In mid-June, when the monsoon starts, the temperature starts falling. It is within the range from 10.5 °C to 6.1 °C from November to February during the winter season. Annual rainfall is about 1200 mm. About 84% of this figure falls within the monsoon season and the rest are in non-monsoon periods. Maximum precipitation occurs in the Himalayan foothills and decreases gradually while

shifting towards the south. In the summer, the mean monthly wind speed is highest in May and June, corresponding to 7.4 and 7.2 km/h, and it decreases to its minimum in October (2.6 km/h).

3. Materials and Methods

The flowchart corresponding to the methodology to estimate spatial surface runoff is illustrated in Figure 2. Different inputs to the models were prepared in raster format to analyze spatial and temporal zonal effects. The study has considered temporal variation since 1981, by performing analysis for three years i.e., 1995 (1981–1995), 2010 (1996–2010), and 2018 (2011–18). The analysis for the years 1995 and 2010 have considered and averaged the past 15 years of datasets whereas for the 2018 year, 8 years of past record is considered for evaluation. Thus, the preparation of input variables to estimate the spatial variation in runoff in different years and understand their correlation is described in subsequent subsections.

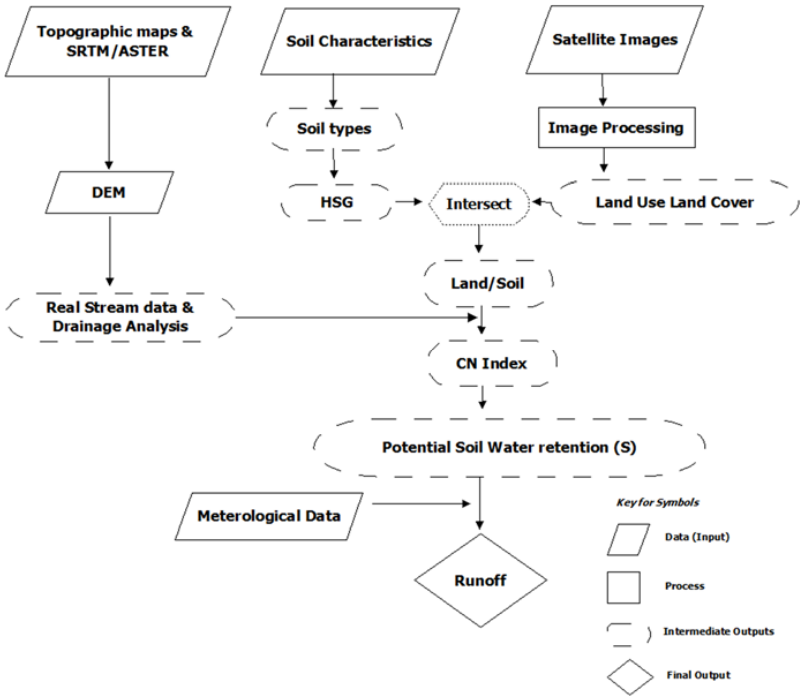

Figure 2. Flowchart of the methodology for the Natural Resources Conservation Service-Curve Number (NRCS-CN) model (Source: Pathak et al. [71]).

3.1. Land Use Land Cover

Landsat images were acquired from the United States Geological Survey (USGS) and clipped according to the extent of the study area for the years 1995, 2010, and 2018. Preprocessing analyses were performed on these images using the ERDAS-Imagine software. The LULC classification was achieved by adopting the nearest neighbor classifier and an object-based image analysis approach. As a result, the study area was classified into seven classes, i.e., water, forest, sand, eroded land, urban, rangeland and agriculture with a spatial resolution of 30 m. The classification was validated using ground truth points and Google Earth images.

3.2. Soil Depth and Texture

The soil map was acquired from the National Bureau of soil survey and land-use planning (NBSSLUP) at a scale of 1:250,000. In grid format, the resolution was resampled from 1200 m to 30 m to achieve the same spatial resolution of LULC using ArcGIS. Different information about the soil is available in the map such as soil depth, slope, percentage of carbon content, texture, temperature,

erosion, drainage, and mineralogy. The required data, viz. soil depth and texture, was transformed into the raster format to perform as an input in the hydrological model.

According to its characteristics, soil is classified into four hydrologic soil groups (HSG), i.e., A, B, C and D. The groups are assigned according to the runoff potential and infiltration capacity of the soil. Groups A to D have high to low infiltration capacity and low to high runoff potential. This parameter assists in computing the composite CN and estimating the fraction of rainfall that flows as surface runoff within a city [72].

3.3. Precipitation and Temperature

The daily series of temperature and precipitation were collected in gridded format with a spatial resolution of 1° and 0.25°, respectively, from the Indian Meteorological Department (IMD). The dataset used in the study is from 1981 to 2018 [73–76].

3.4. Surface Runoff

A combination of the NRCS-CN method with GIS tools was applied to estimate spatial runoff. The NRCS-CN method considers some readily available tables and curves and is based upon a simple empirical formula to obtain surface runoff. The curve number (CN) is an important parameter that influences the estimation of surface runoff. High values of CN represent high amounts of surface runoff and low infiltration capacity of the soil, and vice versa. The CN, which is a function of land use, soil property and slope, was obtained using LULC and soil maps [77].

$$Q = \frac{(P - I_a)^2}{P - I_a + S} \text{ for } P > I_a Q = 0 \text{ for } P \le I_a \quad (1)$$

where Q is direct runoff, P represents total rainfall, S is the potential maximum retention, and I_a is the initial abstraction. I_a is a function of S that can be expressed as

$$I_a = \lambda S \quad (2)$$

Equation (1) becomes,

$$Q = \frac{(P - \lambda S)^2}{P + (1 - \lambda)S} \quad (3)$$

Here, S can be estimated from the P–Q data for a constant value of I_a (0.2 S), and represented in terms of CN using Equation (4).

$$S = \frac{25400}{CN} - 254 \quad (4)$$

The curve number is obtained from three variables: land use land cover, hydrologic soil group (HSG), and antecedent moisture condition (AMC) [72]. Hence, the weighted curve number for the study region can be determined by the following formula.

$$CN_w = \frac{\sum CN_i \times A_i}{A} \quad (5)$$

where CN_w represents the weighted curve number, A is the total area, CN_i is the curve number of sub-catchment i, where sub-catchments (or sub-areas) ranges from 1 to any number N, A_i is the area of sub-catchment i, and N is the total number of sub-catchments in a watershed.

3.5. Annual Water Yield

The InVEST model has the potential to capture the alteration in the flows due to changes in the ecosystem [60]. This model entirely works according to an empirical function derived from the Budyko framework, which provides the ratio of potential evapotranspiration (PET) to actual evapotranspiration

(AET) [78]. The InVEST model captures the spatial variability in precipitation, vegetation, PET, and soil depth to estimate spatial changes in the LULC. The model works on grid format and estimates the heterogeneity in the parameters (LULC, precipitation, temperature, HSG, etc.) affecting the water flows. The spatial water yield is estimated annually for each land use class as follows:

$$Y\left(x\right) = \left(1 - \frac{AET\left(x\right)}{P\left(x\right)}\right) \times P\left(x\right) \tag{6}$$

where, $P(x)$ represents the spatial annual precipitation and $AET(x)$ refers to the actual annual evapotranspiration at each pixel x.

Precipitation and PET determines the mean AET of the watershed. Some of the watershed characteristics, i.e., topography, soil, etc., plays a secondary role. The index of dryness refers to the ratio of annual PET to precipitation to estimate the annual AET.

$$\frac{AET\left(x\right)}{P\left(x\right)} = 1 + \frac{PET\left(x\right)}{P\left(x\right)} - \left[1 + \frac{PET\left(x\right)}{P\left(x\right)}\right]^{\left(\frac{1}{\omega}\right)} \tag{7}$$

where $\omega(x)$ is a non-physical parameter that represents the natural climatic soil properties and PET at each pixel. PET is further estimated by the following expression.

$$PET\left(x\right) = Kc\left(x\right) \times ETo\left(x\right) \tag{8}$$

where $Kc(x)$ represents the vegetation evapotranspiration coefficient, which is a function of the LULC characteristics [79]. Furthermore, ET_0 is the annual reference evapotranspiration, which is determined on the basis of alfalfa grass grown as Equation (11). In addition, $\omega(x)$ is an empirical parameter determined by Donohue et al. [80] as follows.

$$\omega\left(x\right) = z \times \frac{AWC\left(x\right)}{P\left(x\right)} + 1.25 \tag{9}$$

where z is the seasonality factor, the value of which varies from 1 to 30. Further, AWC is a function of the volumetric plant available water content (mm) and is determined through Equation (10).

$$AWC\left(x\right) = Min.\left(\text{Root depth},\ \text{Restricting layer depth}\right) \times PAWC \tag{10}$$

The maximum depth in the soil up to which the roots can penetrate is referred to as root restricting layer depth. Additionally, the depth up to which 95% of the root biomass occurs is defined as root depth. PAWC is the plant available water content, which generally stands for the difference between field capacity and wilting point. ET_o is estimated by the modified Hargreaves method, which is a function of average daily temperature (T_{avg}), temperature range (TD), ET_o, and extraterrestrial radiation (RA). T_{avg} (°C), is the mean of the mean daily maximum and mean daily minimum temperatures, and TD (°C) represents the temperature range obtained as the difference between the mean daily maximum and daily minimum temperatures.

$$ET_o = 0.0013 \times 0.408 \times RA \times \left(T_{avg} + 17.0\right) \times \left(TD - 0.0123 \times P\right)^{0.76} \tag{11}$$

To estimate RA, the expression is given as follows:

$$RA = \frac{24(60)}{\pi} \times G_{sc} \times d_r \times \left[w_s \sin(\varphi) \sin(\delta) + \cos(\varphi) \cos(\delta) \sin(w_s)\right] \tag{12}$$

where d_r is the inverse relative distance Earth–Sun, RA is extraterrestrial radiation [MJm^{-2} d^{-1}], G_{sc} is a solar constant equal to 0.0820 MJm^{-2} min^{-1}, δ is solar declination (rad), w_s is sunset hour angle (rad) and φ is latitude (rad).

In the present study, this approach was utilized to validate the CN based water yield estimates. The InVEST model was applied to understand the spatiotemporal trend of annual water yield with runoff. Moreover, it enables validating both the range and the spatial variation of temporal runoff for the selected years. Further, it provides a second base to deploy decision planning based on spatial water availability within the study area.

4. Results and Discussion

4.1. Supervised Classification

The LULC classification for the study period was obtained using supervised classification, as represented in Figure 3. The study area was divided into seven classes, i.e., forest, water, sand, eroded land, urban, rangeland and agriculture. Table 1 reveals the percentage area covered by each class for the years 1995, 2010 and 2018.

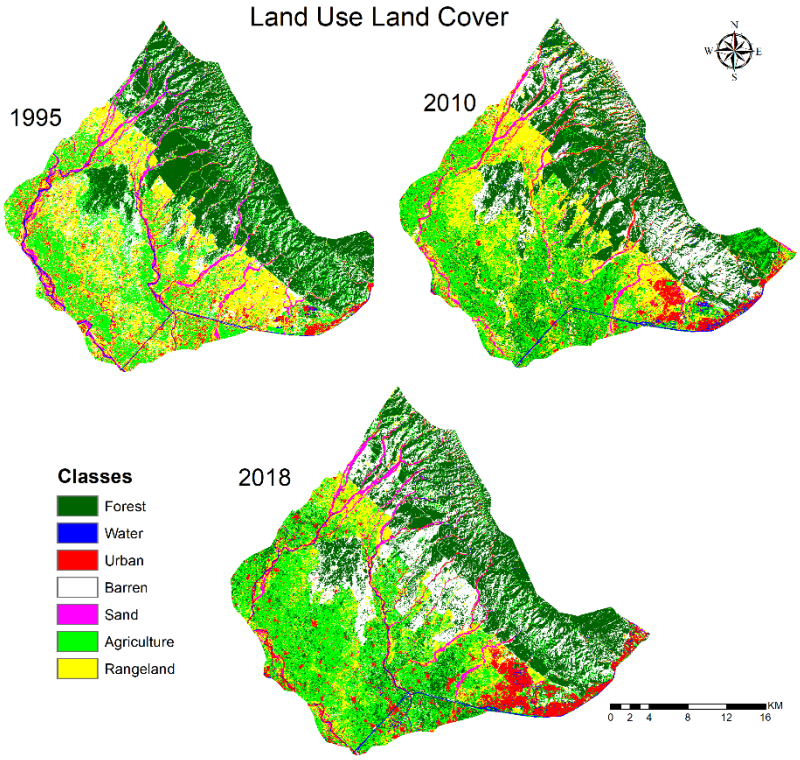

Figure 3. Land Use/Land Cover (LULC) map of the study area for the years 1995, 2010 and 2018.

Table 1. Classification of land-use classes for the years 1995, 2010 and 2018.

Class	Percentage (1995)	Percentage (2010)	Percentage (2018)
Forest	29.57	30.68	28.12
Water	1.37	1.43	1.51
Eroded land	18.32	18.11	21.26
Sand	3.73	2.21	2.38
Urban	5.5	6.3	8.71
Rangeland	20.34	19.76	11.23
Agriculture	20.02	21.53	26.79

From Table 1, it is understood that a large part of the study area is covered under forest, which is approximately 30% of the total area (254 sq. km). The upper Siwalik region is covered with forest and some built-up areas that include urban forests. Agriculture and rangeland extends to approximately 40%, as agriculture is a major occupation in this region. Water bodies account for approximately 1.4% of the total area since 1995. Most of this water is transmitted through the canal in the study area, with some small ponds and lakes situated near the residential area. The flashy stream contains water only in the monsoon season. Eroded land is formed due to the erosion of the surface caused by high discharge. The slopes are steep (more than 12%) and streams contain large flows in the monsoon season. To verify the accuracy of this supervised classification, an accuracy assessment was performed as tabulated in Table 2. User accuracy corresponds to the error of commission whereas producer accuracy defines the error of omission in the LULC classification. In other words, user accuracy is the ratio of the number of pixels correctly identified to the number of pixels claimed to be in the respective maps class. The producer accuracy is the ratio of the number of pixels correctly identified in reference plots to the number actually in that reference class. Thus, user and producer accuracy were computed for each class of the study area as described in Table 2.

Table 2. Accuracy assessment of supervised classification for the years 1995, 2010 and 2018.

LULC Classes	1995		2010		2018	
	Producer Accuracy (%)	**User Accuracy (%)**	**Producer Accuracy (%)**	**User Accuracy (%)**	**Producer Accuracy (%)**	**User Accuracy (%)**
Forest	74.35	82.85	76.38	83.65	77.52	83.36
Wasteland	74.36	82.85	77.36	82.36	74.25	82.14
Rangeland	78.94	85.71	77.69	86.32	79.69	86.31
Agriculture	79.82	85.71	81.23	86.36	79.36	85.10
Built up	84.84	80.00	85.36	78.36	84.69	81.23
Sand	72.97	77.84	73.25	79.32	73.36	79.25
Water	84.00	60.00	85.36	72.00	85.00	65.00

4.2. Trend Analysis of Land Cover Classes

The trend analysis chart is shown in Figure 4. It shows that the forest area reduced from 29.57% (250.46 sq. km) in 1995 to 28.12% (238.176 sq. km) in 2018. The change in forest area is not significant as compared to the increased urban area because of the policies strategized by the government to protect forest. Water class has remained constant since 1995, because most of the water demand is met by the canal. Very little change is observed in the water class as the water flows in the flashy streams. Built-up area increased from 5.5%, (46.58 sq. km) in 1995 to 8.71%, (73.77 sq. km) in 2018. Most of the urbanization is in the lower Siwalik and the plain region. Total cultivable land, which was approximately 40% in 1995, also decreased and became 38% in the year 2018, representing urbanization as directly proportional to cultivation. The eroded land increased by approximately 3% of the area directing the influence of flashy streams and anthropogenic activities in the area. Moreover, the region experienced high sediment loads, which makes it more vulnerable to flood risk. Thus, suitable low impact development (LID) techniques should be implemented at specified zones to mitigate potential negative impacts and prevent socio-economic loss.

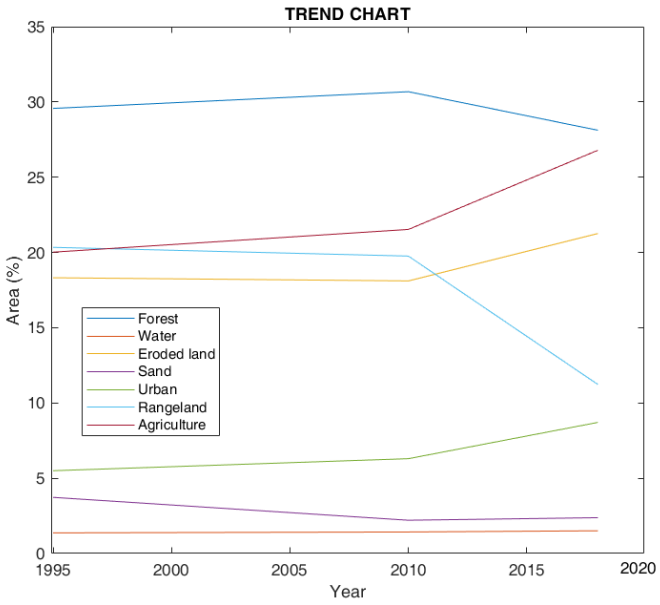

Figure 4. Trend chart of LULC for the study area from 1995 to 2018.

4.3. Curve Number Analysis

Once the raster map was prepared for the soil and LULC, the maps were integrated into the ArcGIS environment to create the curve number map. Hence, the curve number maps obtained for the study area are represented in Figure 5. The higher value of curve number defines the higher runoff for that particular zone and vice versa. The results portray a clear picture of the zones that are experiencing high surface runoff. Thus, to handle drought and flooding situations, water harvesting schemes should be implemented in these specific areas having an abundant amount of surface water availability. In this scenario, the zones having higher CN value represents potential suitable sites for water harvesting.

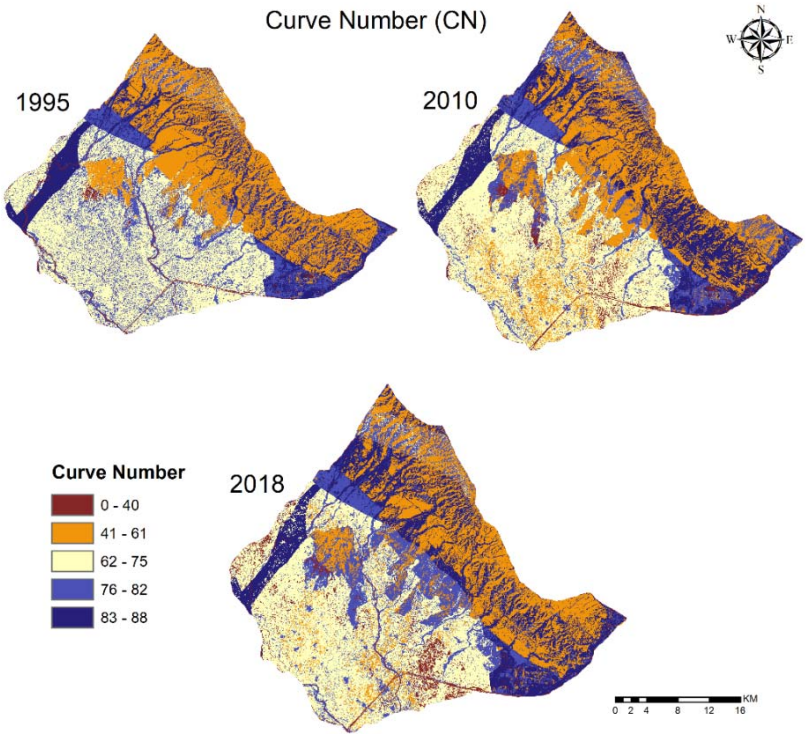

Figure 5. Curve number map of the study area.

4.4. Variation in Area Ratio

The curve number is a function of the LULC and soil property of the area. Figure 6 shows the spatial distribution of the CN during the years 1995, 2010 and 2018. Area ratio represents the ratio of a particular land covered with a specific number of CN values to the total area. It is understood from Figure 6 that the CN is increasing from 1995 to 2018. The initial range of CN (26–61) belongs to the forest area, which is decreasing from 1995 to 2018. The agriculture and crop areas are also reduced, and the maximum deviation in the CN is in the range of 83–87, which belongs to wasteland and built up area. A decrease in forest and cultivated land and an increase in wasteland and built-up area are observed in the city due to the effect of urban sprawl.

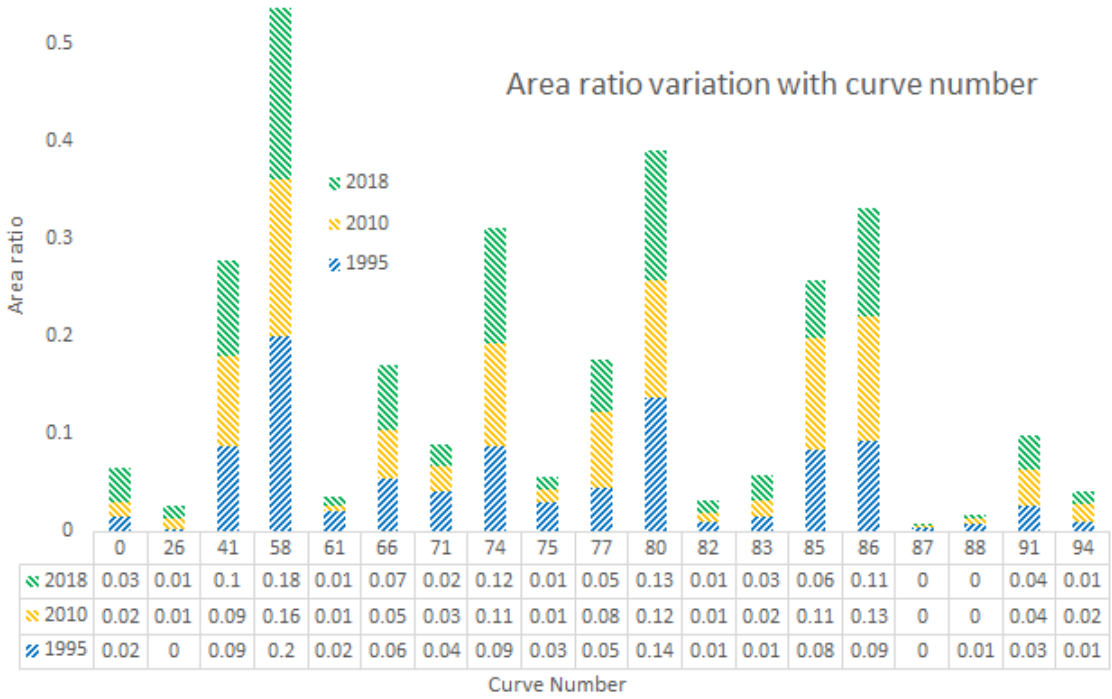

	0	26	41	58	61	66	71	74	75	77	80	82	83	85	86	87	88	91	94
2018	0.03	0.01	0.1	0.18	0.01	0.07	0.02	0.12	0.01	0.05	0.13	0.01	0.03	0.06	0.11	0	0	0.04	0.01
2010	0.02	0.01	0.09	0.16	0.01	0.05	0.03	0.11	0.01	0.08	0.12	0.01	0.02	0.11	0.13	0	0	0.04	0.02
1995	0.02	0	0.09	0.2	0.02	0.06	0.04	0.09	0.03	0.05	0.14	0.01	0.01	0.08	0.09	0	0.01	0.03	0.01

Figure 6. Variation of area ratio with Curve Number for the years 1995, 2010 and 2018.

4.5. Runoff Analysis

Monthly runoff was estimated for the study area by providing rainfall data as an input to the NRCS-CN method, as represented in Figure 7. For the year 1995, maximum rainfall was observed in August, which corresponds to AMC III condition and a maximum amount of runoff for this period. About 85% of the yearly rainfall is observed in July to August, contributing to maximum runoff in these months. AMC I condition exists for the rest of the months, as they received less rainfall and thus resulted in a lower amount of runoff. Thus, an adjustment table was referred to select the curve number corresponding to different soil moisture conditions [81].

For the year 2010, the area receives a lower amount of rainfall in the non-monsoon period, whilst approximately 87% of total rainfall occurs during the monsoon period. The AMC III condition is applicable for the monsoon region, thereby causing a higher amount of runoff in this period. Some of the rainfall is observed in the winter season due to the western disturbances, but runoff is nearly zero because of the non-saturation condition of the soil. As for 2018, rainfall is very low as compared to previous years. Because of the lesser rainfall in the area, the AMC II condition is applicable for June, July and August. Hence, the estimated runoff is also very reduced in relation to previous years.

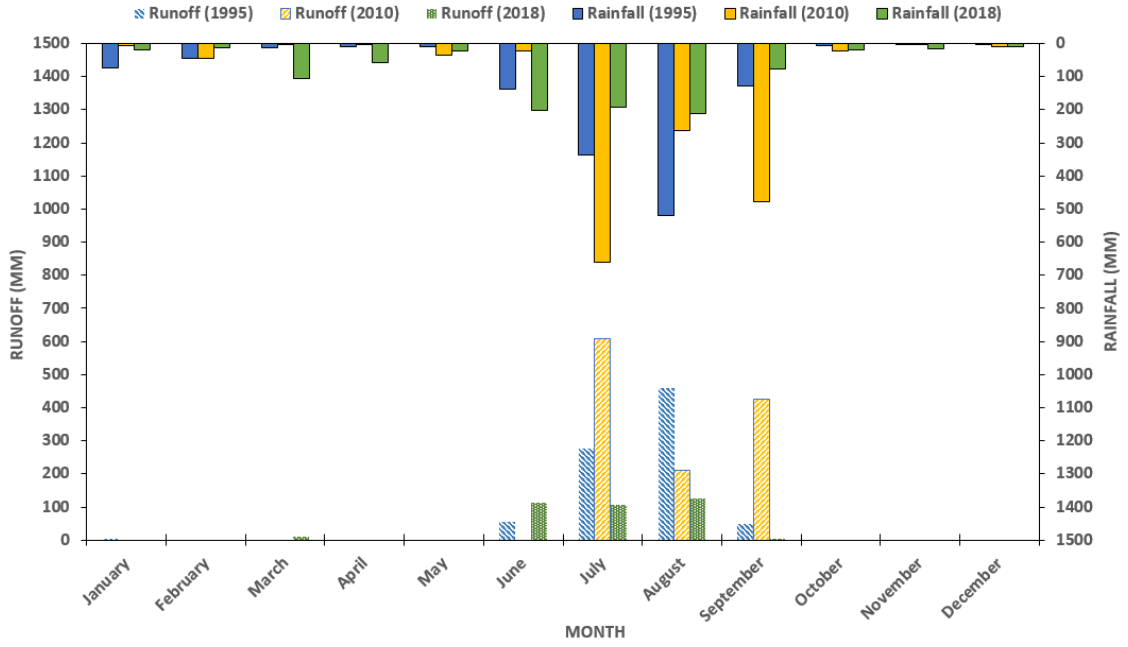

Figure 7. Rainfall and runoff variation in the study region for the years 1995, 2010 and 2018.

The observed mean annual rainfall for the Haridwar district is approximately 1174.3 mm, which is also 85% of the rainfall observed for the monsoon period, i.e., from July to September. Out of the three years under study, 2010 was found to receive the maximum amount of rainfall and runoff, as shown in Figure 7. As the data of the Ganges basin is classified, it is challenging to present the complete results along with their validation in the paper.

The computation was performed to analyze the impact of climate change and anthropogenic activities on the regional surface runoff potential. The study infers that runoff increased approximately 48% from 1995 to 2010 and 71% from 2010 to 2018 (Figure 8). The values of weighted CN are 69.24, 70.96 and 71.24 for 1995, 2010 and 2018, respectively.

The CN values were found to have very little temporal variability for the study area (Figure 7). This suggested that LULC, soil map or variations in land-use class have low influence on surface runoff. Changes in the rainfall pattern and intensity are solely responsible for the flooding condition in the study region. The city experiences runoff mainly during July to September. In July, runoff was maximum in 2010 (approximately 100% greater than in 1995 and 245% greater than in 2018). Subsequently, flooding can be mitigated by implementing water harvesting schemes at the specified areas that experience high surface runoff. Furthermore, to validate the annual spatial trend of runoff, the InVEST model is applied to estimate the annual water yield.

4.6. Validation Using Alternative Approach

The Himalayan study region has very little data available for validation due to the political restriction and physical difficulties. The mountainous region of the Himalayas are not equipped with any gauging stations. The downstream of the catchment has measuring stations available. However, due to the data sharing constrained by government policies, it is very difficult to validate the model with the observation stations. This results in a lack of data availability for the research community resulting in little hydrological and water resources analysis in the Ganges basin.

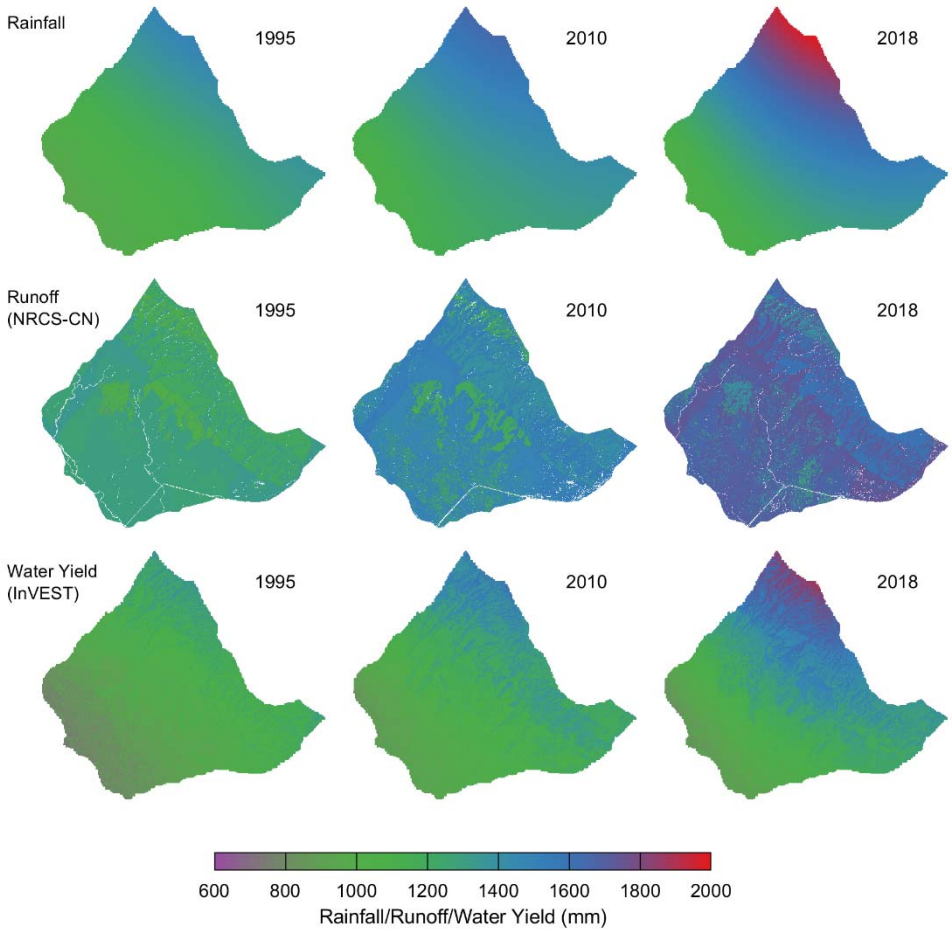

Figure 8. Validation of annual surface runoff model with annual water yield model.

Therefore, to capture and validate the spatial trend of runoff estimated by the NRCS-CN model, the InVEST model was applied to the study region. The annual spatiotemporal variations in water yield (InVEST) and surface runoff (NRCS-CN) are represented in Figure 8. It has been observed that the range of yield and runoff for the selected years are similar; however, they vary in their spatial trend. This is a very interesting finding, whereby both approaches show spatial variability of runoff and yield despite the similarity of yield and runoff in different years. Due to the variation in the Budyko and CN approaches, different classes represent different runoff potential with the same range of surface runoff for all the selected years.

However, low temporal variations are observed in the weighted curve number values between the selected years. Therefore, yield or runoff entirely depend upon the rainfall trend of the study region. To understand and deploy site specific strategic planning, it is required to analyze the monthly variation and trend of rainfall. Thus, monthly rainfall data was observed and analyzed effectively for decision-making and policy purposes. The monthly analysis provides a clear assessment of surface water runoff for the three selected years. It has been observed that the city experiences high rainfall in July, August and September which results in high surface runoff and flooding conditions. By considering the importance of the city, proper management of water resources should be strategized for the specified months based on the CN analysis, which provides a detailed assessment and location of the zones that are vulnerable to high surface runoff.

Furthermore, the study indicated that most of the months remain dry. Thus, the city will depend on natural resources or storage tanks for potable and non-potable water demands. If the storage tanks are constructed and utilized during rainfall periods, they can be used to store water for dry months and thus reduce the exploitation of natural resources. In this context, it is recommended to

implement stormwater harvesting schemes and storage tanks in the desired zones. This course of action will address the increasing demand and low water resources availability, making water accessible for inhabitants and civilians. Geospatial tools can assist in obtaining more precise information in rainfall-runoff modeling about the catchment size and characteristics. Further, the analysis can be performed swiftly by integrating composite land-use classes with diverse soil types. Thus, effective planning can be deployed at the sites of interest to have an abundant availability of supply during dry periods. Additionally, awareness programs can be targeted at specified zones for water conservation and mitigating disasters such as floods and droughts.

5. Conclusions

Estimation of surface runoff helps in sustainable planning and management of land use and available water content. Towards this, the NRCS-CN method was initially applied for estimating the regional composite curve number. The present methodology reduces time as well as the efforts to deploy strategic planning by focusing on spatial water availability. The method also yields comparable estimates as those obtained using the Budyko model. However, the spatial variability of water yield is observed in both approaches. It has been analyzed that the city has not experienced much temporal variation in the weighted curve number since 1995. In other words, changes in land use and topography due to the anthropogenic influences since 1995 will not have much influence on flow variability. Hence, runoff is directly proportional to rainfall, which has substantially changed due to the effect of climate change. Thus, the implementation of suitable conservation practices and structural works is suggested to reduce the pressure from freshwater resources within the city. As a fact, cities are facing natural calamities very often due to urban sprawl, such as droughts or flooding. Nevertheless, if suitable zones are identified and combined with the knowledge of water availability and demand, strategic plans can be deployed spatially with ease. Additionally, if the conservation practices are suitably placed, urban flooding can be embraced as an opportunity to treat the regions with water demands during dry periods. Henceforth, it is highly recommended to implement some low impact development techniques within the zones with high water availability, so that the dependency on natural resources is reduced and the effect of disaster could be mitigated with time.

Author Contributions: Conceptualization, S.P. and D.J.-E.; methodology, S.P., C.S.P.O. and R.D.G.; validation, S.P.; formal analysis, S.P. and D.J.-E.; writing—original draft preparation, S.P. and C.S.P.O.; writing—review and editing, D.J.-E., R.D.G., M.L., R.P.S.; supervision, C.S.P.O., R.D.G. and M.L. All authors have read and agreed to the published version of the manuscript.

Funding: The authors are thankful to the National Key R&D Program of China (2017YFE0100700), Ministry of Science and Technology (MOST), China, for providing the required funds to support this research.

Acknowledgments: The authors are thankful to the China Postdoctoral Science Foundation, China for providing the required funds and support. The authors are thankful to Central Ground Water Board (CGWB), Dehradun and Indian Meteorological Department (IMD), India, for providing the needful data to carry out the study for the Haridwar region, Uttarakhand.

Conflicts of Interest: The authors declare no conflict of interest.

References

1. Anderson, J.R.; Hardy, E.E.; Roach, J.T.; Witmer, R.E. *A Land Use and Land Cover Classification System for Use with Remote Sensor Data*; U.S. Geological Survey Professional Paper, No. 964; USGS: Washington, DC, USA, 1976.
2. Mishra, S.K.; Singh, V.P. *Soil Conservation Service Curve Number (SCS-CN) Methodology*; Springer: Berlin/Heidelberg, Germany, 2013; Volume 42.
3. Mishra, S.K.; Sahu, R.K.; Eldho, T.I.; Jain, M.K. An improved IaS relation incorporating antecedent moisture in SCS-CN methodology. *Water Resour. Manag.* **2006**, *20*, 643–660. [CrossRef]
4. Hu, S.; Fan, Y.; Zhang, T. Assessing the effect of land use change on surface runoff in a rapidly urbanized city: A case study of the central area of Beijing. *Land* **2020**, *9*, 17. [CrossRef]

5. Luo, J.; Zhou, X.; Rubinato, M.; Li, G.; Tian, Y.; Zhou, J. Impact of multiple vegetation covers on surface runoff and sediment yield in the small basin of Nverzhai, Hunan province, China. *Forests* **2020**, *11*, 329. [CrossRef]
6. Qi, J.; Lee, S.; Zhang, X.; Yang, Q.; McCarty, G.W.; Moglen, G.E. Effects of surface runoff and infiltration partition methods on hydrological modeling: A comparison of four schemes in two watersheds in the Northeastern US. *J. Hydrol.* **2020**, *581*, 124415. [CrossRef]
7. Shrivastav, M.; Mickelson, S.K.; Webber, D. Using ArcGIS hydrologic modeling and LiDAR digital elevation data to evaluate surface runoff interception performance of riparian vegetative filter strip buffers in central Iowa. *J. Soil Water Conserv.* **2020**, *75*, 123–129. [CrossRef]
8. Xu, C.; Rahman, M.; Haase, D.; Wu, Y.; Su, M.; Pauleit, S. Surface runoff in urban areas: The role of residential cover and urban growth form. *J. Clean. Prod.* **2020**, *262*, 121421. [CrossRef]
9. Steenhuis, T.S.; Winchell, M.; Rossing, J.; Zollweg, J.A.; Walter, M.F. SCS runoff equation revisited for variable-source runoff areas. *J. Irrig. Drain. Eng.* **1995**, *121*, 234–238. [CrossRef]
10. Van Dijk, A.I.J.M. Selection of an appropriately simple storm runoff model. *Hydrol. Earth Syst. Sci.* **2010**, *14*, 447. [CrossRef]
11. Abon, C.C.; David, C.P.C.; Pellejera, N.E.B. Reconstructing the tropical storm Ketsana flood event in Marikina river, Philippines. *Hydrol. Earth Syst. Sci.* **2011**, *15*, 1283. [CrossRef]
12. Soil Conservation Service (SCS). *Hydrology, National Engineering Handbook*; Soil Conservation Service, USDA: Washington, DC, USA, 1985.
13. Shrestha, M.N. Spatially distributed hydrological modeling considering land-use changes using remote sensing and GIS. In Proceedings of the Map Asia Conference, Kuala Lumpur, Malaysia, 13–15 October 2003; pp. 1–8.
14. Zhan, X.; Huang, M.L. ArcCN-Runoff: An ArcGIS tool for generating curve number and runoff maps. *Environ. Model. Softw.* **2004**, *19*, 875–879. [CrossRef]
15. Mishra, S.K.; Jain, M.K.; Singh, V.P. Evaluation of the SCS-CN-based model incorporating antecedent moisture. *Water Resour. Manag.* **2004**, *18*, 567–589. [CrossRef]
16. Soulis, K.X.; Valiantzas, J.D. SCS-CN parameter determination using rainfall-runoff data in heterogeneous watersheds-the two-CN system approach. *Hydrol. Earth Syst. Sci.* **2012**, *16*, 1001. [CrossRef]
17. Ghate, A.S. Rainfall runoff modeling using SCS-CN method: A GIS based case study of Pawana watershed. *J. Water Resour. Eng. Manag.* **2019**, *3*, 50–58.
18. Pishvaei, M.H.; Sabzevari, T.; Noroozpour, S.; Mohammadpour, R. Effects of hillslope geometry on spatial infiltration using the TOPMODEL and SCS-CN models. *Hydrolog. Sci. J.* **2020**, *65*, 212–226. [CrossRef]
19. Walega, A.; Amatya, D.M.; Caldwell, P.; Marion, D.; Panda, S. Assessment of storm direct runoff and peak flow rates using improved SCS-CN models for selected forested watersheds in the Southeastern United States. *J. Hydrol. Reg. Stud.* **2020**, *27*, 100645. [CrossRef]
20. Hjelmfelt, A.T., Jr. Investigation of curve number procedure. *J. Hydraul. Eng.* **1991**, *117*, 725–737. [CrossRef]
21. Hawkins, R.H. Asymptotic determination of runoff curve numbers from data. *J. Irrig. Drain. Eng.* **1993**, *119*, 334–345. [CrossRef]
22. Grove, M.; Harbor, J.; Engel, B. Composite vs. distributed curve numbers: Effects on estimates of storm runoff depths. *J. Am. Water Resour. Assoc.* **1998**, *34*, 1015–1023. [CrossRef]
23. Moglen, G.E. Effect of orientation of spatially distributed curve numbers in runoff calculations. *J. Am. Water Resour. Assoc.* **2000**, *36*, 1391–1400. [CrossRef]
24. Farran, M.M.; Elfeki, A.M. Evaluation and validity of the antecedent moisture condition (AMC) of Natural Resources Conservation Service-Curve Number (NRCS-CN) procedure in undeveloped arid basins. *Arab. J. Geosci.* **2020**, *13*, 275. [CrossRef]
25. Lian, H.; Yen, H.; Huang, C.; Feng, Q.; Qin, L.; Bashir, M.A.; Wu, S.; Zhu, A.X.; Luo, J.; Di, H.; et al. CN-China: Revised runoff curve number by using rainfall-runoff events data in China. *Water Res.* **2020**, *177*, 115767. [CrossRef] [PubMed]
26. Ormsbee, L.; Hoagland, S.; Peterson, K. Limitations of TR-55 curve numbers for urban development applications: Critical review and potential strategies for moving forward. *J. Hydrol. Eng.* **2020**, *25*, 02520001. [CrossRef]
27. Rao, K.N. Analysis of surface runoff potential in ungauged basin using basin parameters and SCS-CN method. *Appl. Water Sci.* **2020**, *10*, 47.

28. Hassaballah, K.; Mohamed, Y.; Uhlenbrook, S.; Biro, K. Analysis of streamflow response to land use and land cover changes using satellite data and hydrological modelling: Case study of Dinder and Rahad tributaries of the Blue Nile (Ethiopia–Sudan). *Hydrol. Earth Syst. Sci.* **2017**, *21*, 5217. [CrossRef]
29. Pathak, S.; Ojha, C.S.P.; Garg, R.D.; Lakshmi, V. Urbanization and Its Impact on Stormwater Runoff Potential Using Geospatial Tools. In Proceedings of the Geoscience and Remote Sensing Symposium (IGARSS), Valencia, Spain, 22–27 July 2018.
30. Lal, M.; Mishra, S.K.; Pandey, A.; Pandey, R.P.; Meena, P.K.; Chaudhary, A.; Jha, R.K.; Shreevastava, A.K.; Kumar, Y. Evaluation of the soil conservation service curve number methodology using data from agricultural plots. *Hydrogeol. J.* **2017**, *25*, 151–167. [CrossRef]
31. Bonta, J.V. Determination of watershed curve number using derived distributions. *J. Irrig. Drain. Eng.* **1997**, *123*, 28–36. [CrossRef]
32. Farran, M.M.; Elfeki, A.M. Statistical analysis of NRCS curve number (NRCS-CN) in arid basins based on historical data. *Arab. J. Geosci.* **2020**, *13*, 151–167.
33. Lee, H.K.; Lee, K.H. Impact of representative SCS-CN on simulated rainfall runoff. *J. Environ. Sci. Int.* **2020**, *29*, 25–32. [CrossRef]
34. Shi, W.; Wang, N. An improved SCS-CN method incorporating slope, soil moisture, and storm duration factors for runoff prediction. *Water* **2020**, *12*, 1335. [CrossRef]
35. Xu, A.L. A new curve number calculation approach using GIS technology. In Proceedings of the ESRI 26th International User Conference on Water Resources, San Diego, CA, USA, 7–11 August 2006.
36. Satheeshkumar, S.; Venkateswaran, S.; Kannan, R. Rainfall–runoff estimation using SCS–CN and GIS approach in the Pappiredipatti watershed of the Vaniyar sub basin, South India. *Model. Earth Sys. Environ.* **2017**, *3*, 24. [CrossRef]
37. Singh, L.K.; Jha, M.K.; Chowdary, V.M. Multi-criteria analysis and GIS modeling for identifying prospective water harvesting and artificial recharge sites for sustainable water supply. *J. Clean. Prod.* **2017**, *142*, 1436–1456. [CrossRef]
38. Ling, L.; Yusop, Z.; Yap, W.S.; Tan, W.L.; Chow, M.F.; Ling, J.L. A calibrated, watershed-specific SCS-CN method: Application to Wangjiaqiao watershed in the three Gorges area, China. *Water* **2020**, *12*, 60. [CrossRef]
39. Rajasekhar, M.; Gadhiraju, S.R.; Kadam, A.; Bhagat, V. Identification of groundwater recharge-based potential rainwater harvesting sites for sustainable development of a semiarid region of southern India using geospatial, AHP, and SCS-CN approach. *Arab. J. Geosci.* **2020**, *13*, 24. [CrossRef]
40. Shi, W.; Wang, N. Improved SMA-based SCS-CN method incorporating storm duration for runoff prediction on the Loess Plateau, China. *Hydrol. Res.* **2020**, *51*, 443–455. [CrossRef]
41. Soulis, K.X.; Valiantzas, J.D.; Dercas, N.; Londra, P.A. Analysis of the runoff generation mechanism for the investigation of the SCS-CN method applicability to a partial area experimental watershed. *Hydrol. Earth Syst. Sci.* **2009**, *13*, 605–615. [CrossRef]
42. Rezaei-Sadr, H. Influence of coarse soils with high hydraulic conductivity on the applicability of the SCS-CN method. *Hydrol. Sci. J.* **2017**, *62*, 843–848. [CrossRef]
43. Al-Juaidi, A.E.M. A simplified GIS-based SCS-CN method for the assessment of land-use change on runoff. *Arab. J. Geosci.* **2018**, *11*, 269. [CrossRef]
44. Arya, S.; Subramani, T.; Karunanidhi, D. Delineation of groundwater potential zones and recommendation of artificial recharge structures for augmentation of groundwater resources in Vattamalaikarai Basin, South India. *Environ. Earth Sci.* **2020**, *79*, 102. [CrossRef]
45. Al-Ghobari, H.; Dewidar, A.; Alataway, A. Estimation of Surface Water Runoff for a Semi-Arid Area Using RS and GIS-Based SCS-CN Method. *Water* **2020**, *12*, 1924. [CrossRef]
46. Karunanidhi, D.; Anand, B.; Subramani, T.; Srinivasamoorthy, K. Rainfall-surface runoff estimation for the Lower Bhavani basin in south India using SCS-CN model and geospatial techniques. *Environ. Earth Sci.* **2020**, *79*, 335. [CrossRef]
47. Nayak, T.R.; Jaiswal, R.K. Rainfall-runoff modelling using satellite data and GIS for Bebas river in Madhya Pradesh. *J. Inst. Eng. India* **2003**, *84*, 47–50.
48. Geena, G.B.; Ballukraya, P.N. Estimation of runoff for Red hills watershed using SCS method and GIS. *Indian J. Sci. Technol.* **2011**, *4*, 899–902. [CrossRef]
49. Gitika, T.; Ranjan, S. Estimation of surface runoff using NRCS curve number procedure in Buriganga Watershed, Assam, India-a geospatial approach. *Int. Res. J. Earth Sci.* **2014**, *2*, 1–7.

50. Ajmal, M.; Kim, T.W. Quantifying excess stormwater using SCS-CN–based rainfall runoff models and different curve number determination methods. *J. Irrig. Drain. Eng.* **2015**, *141*, 04014058. [CrossRef]
51. Jha, M.K.; Chowdary, V.M.; Kulkarni, Y.; Mal, B.C. Rainwater harvesting planning using geospatial techniques and multicriteria decision analysis. *Resour. Conserv. Recycl.* **2014**, *83*, 96–111. [CrossRef]
52. Bhaskar, J.; Suribabu, C.R. Estimation of surface run-off for urban area using integrated remote sensing and GIS approach. *Jordan J. Civ. Eng.* **2014**, *8*, 70–80. [CrossRef]
53. Dinagara Pandi, P.; Saravanan, K.; Mohan, K. Identifying runoff harvesting sites over the Pennar Basin, Andhra pradesh using SCS-CN method. *Int. J. Civ. Eng. Technol.* **2017**, *8*, 65–73.
54. Karunanidhi, D.; Aravinthasamy, P.; Subramani, T.; Roy, P.D.; Srinivasamoorthy, K. Risk of fuoride-rich groundwater on human health: Remediation through managed aquifer recharge in a hard rock terrain, South India. *Nat. Resour. Res.* **2019**, *29*, 2369–2395. [CrossRef]
55. Tallis, H.T.; Ricketts, T.; Nelson, E.; Ennaanay, D.; Wolny, S.; Olwero, N.; Vigerstol, K.; Pennington, D.; Mendoza, G.; Aukema, J.; et al. *InVEST 1.004 Beta User's Guide*; The Natural Capital Project: Stanford, CA, USA, 2010.
56. Shukla, A.K.; Pathak, S.; Pal, L.; Ojha, C.S.P.; Mijic, A.; Garg, R.D. Spatio-temporal assessment of annual water balance models for upper Ganga Basin. *Hydrol. Earth Syst. Sci.* **2018**, *22*, 5357–5371. [CrossRef]
57. Terrado, M.; Acuña, V.; Ennaanay, D.; Tallis, H.; Sabater, S. Impact of climate extremes on hydrological ecosystem services in a heavily humanized Mediterranean basin. *Ecol. Indic.* **2014**, *37*, 199–209. [CrossRef]
58. Hoyer, R.; Chang, H. Assessment of freshwater ecosystem services in the Tualatin and Yamhill basins under climate change and urbanization. *Appl. Geogr.* **2014**, *53*, 402–416. [CrossRef]
59. Thellmann, K.; Blagodatsky, S.; Häuser, I.; Liu, H.; Wang, J.; Asch, F.; Cadisch, G.; Cotter, M. assessing ecosystem services in rubber dominated landscapes in south-east Asia—A challenge for biophysical modeling and transdisciplinary valuation. *Forests* **2017**, *8*, 505. [CrossRef]
60. Pathak, S.; Ojha, C.S.P.; Shukla, A.K.; Garg, R.D. Assessment of Annual Water-Balance Models for Diverse Indian Watersheds. *J. Sustain. Water Built Environ.* **2019**, *5*, 04019002. [CrossRef]
61. Pathak, S.; Ojha, C.S.P.; Zevenbergen, C.; Garg, R.D. Assessing Stormwater Harvesting Potential in Dehradun City Using Geospatial Technology. In *Development of Water Resources in India*; Springer: Cham, Switzerland, 2017; pp. 47–60.
62. Pathak, S.; Ojha, C.S.P.; Zevenbergen, C.; Garg, R.D. Ranking of storm water harvesting sites using heuristic and non-heuristic weighing approaches. *Water* **2017**, *9*, 710. [CrossRef]
63. Lee, J.Y.; Kim, N.W.; Kim, T.W.; Jehanzaib, M. Feasible ranges of runoff curve numbers for Korean watersheds based on the interior point optimization algorithm. *KSCE J. Civ. Eng.* **2019**, *23*, 5257–5265. [CrossRef]
64. Jiao, P.; Xu, D.; Li, B.; Yu, Y. A modified Ia-S relationship improves runoff prediction of the USDA-NRCS curve number model. *T. ASABE* **2019**, *62*, 771–778. [CrossRef]
65. Singh, P.; Mishra, S. Determination of curve number and estimation of runoff using Indian experimental rainfall and runoff data. *J. Spat. Hydrol.* **2019**, *13*, 1–26.
66. Zhang, W.Y. Application of NRCS-CN method for estimation of watershed runoff and disaster risk. *Geomat. Nat. Hazards Risk* **2019**, *10*, 2220–2238. [CrossRef]
67. Kastridis, A.; Stathis, D. Evaluation of Hydrological and Hydraulic Models Applied in Typical Mediterranean Ungauged Watersheds Using Post-Flash-Flood Measurements. *Hydrology* **2020**, *7*, 12. [CrossRef]
68. Kastridis, A.; Kirkenidis, C.; Sapountzis, M. An integrated approach of flash flood analysis in ungauged Mediterranean watersheds using post-flood surveys and Unmanned Aerial Vehicles (UAVs). *Hydrol. Process.* **2020**. [CrossRef]
69. Nastiti, K.D.; An, H.; Kim, Y.; Jung, K. Large-scale rainfall–runoff–inundation modeling for upper Citarum River watershed, Indonesia. *Environ. Earth Sci.* **2018**, *77*, 640. [CrossRef]
70. Pathak, S.; Garg, R.D.; Jato-Espino, D.; Lakshmi, V.; Ojha, C.S.P. Evaluating hotspots for stormwater harvesting through participatory sensing. *J. Environ. Manag.* **2019**, *242*, 351–361. [CrossRef] [PubMed]
71. Pathak, S.; Liu, M.; Jato-Espino, D.; Zevenbergen, C. Social, economic and environmental assessment of urban sub-catchment flood risks using a multi-criteria approach: A case study in Mumbai City, India. *J. Hydrol.* **2020**, *591*, 125216. [CrossRef]
72. Mishra, S.K.; Jain, M.K.; Pandey, R.P.; Singh, V.P. Catchment area-based evaluation of the AMC-dependent SCS-CN-based rainfall–runoff models. *Hydrol. Process.* **2005**, *19*, 2701–2718. [CrossRef]

73. Rahman, H.; Sengupta, D. *Preliminary Comparison of Daily Rainfall from Satellites and Indian Gauge Data*; CAOS Technical Report, (2007AS1); Indian Institute of Science: Bangalore, India, 2007.
74. Singh, A.K.; Tripathi, J.N.; Singh, K.K.; Singh, V.; Sateesh, M. Comparison of different satellite-derived rainfall products with IMD gridded data over Indian meteorological subdivisions during Indian Summer Monsoon (ISM) 2016 at weekly temporal resolution. *J. Hydrol.* **2019**, *575*, 1371–1379. [CrossRef]
75. Kumar, T.V.L.; Barbosa, H.A.; Thakur, M.K.; Paredes-Trejo, F. Validation of satellite (TMPA and IMERG) rainfall products with the IMD gridded data sets over monsoon core region of India. In *Satellite Information Classification and Interpretation*; IntechOpen: Rijeka, Croatia, 2019.
76. Jena, P.; Garg, S.; Azad, S. Performance Analysis of IMD High-Resolution Gridded Rainfall (0.25°× 0.25°) and Satellite Estimates for Detecting Cloudburst Events over the Northwest Himalayas. *J. Hydrometeorol.* **2020**, *21*, 1549–1569. [CrossRef]
77. Ojha, C.S.P.; Bhunya, P.; Berndtsson, R. *Engineering Hydrology*, 1st ed.; Oxford University Press: Oxford, UK, 2008; pp. 1–459.
78. Budyko, M.I.; Ronov, A.B. Evolution of chemical composition of the atmosphere during the Phanerozoic. *Geokhimiya* **1979**, *5*, 643–653.
79. Allen, R.G.; Pereira, L.S.; Raes, D.; Smith, M. *Crop Evapotranspiration-Guidelines for Computing Crop Water Requirements-FAO Irrigation and Drainage Paper 56*; FAO: Rome, Italy, 1998; Volume 300, p. D05109.
80. Donohue, R.J.; Roderick, M.L.; McVicar, T.R. Roots, storms and soil pores: Incorporating key ecohydrological processes into Budyko's hydrological model. *J. Hydrol.* **2012**, *436*, 35–50. [CrossRef]
81. Ward, A.D.; Trimble, S.W. *Environmental Hydrology*; CRC Press: Boca Raton, FL, USA, 2003.